Int. J. Heat Mass Transfer. Vol. 34, No. 7, pp. 1799–1810, 1991
Printed in Great Britain

0017-9310/91 $3.00 + 0.00

Mechanisms of heat and mass transport at gas–liquid interfaces

M. RASHIDI, G. HETSRONI† and S. BANERJEE
Department of Chemical and Nuclear Engineering, University of California, Santa Barbara, CA 93106, U.S.A.

(*Received* 24 *April* 1990 *and in final form* 29 *August* 1990)

Abstract—Interfacial transport in turbulent liquid flows has been studied in a flume. Flow visualization experiments indicate that turbulence structure near boundaries (interface or wall) is governed by the shear rate. For low values of the interfacial shear rate, 'patches' are observed at the interfaces that are formed from the ejections generated near the wall. The ejections are seen to reach the interface, form renewed surface patches, return and mix into the bulk flow. For high values of the interfacial shear rate, the low-speed/high-speed streaks are formed at the interface that break down as 'bursts'. The qualitative features of the streaks and bursts are similar to the ones observed near the wall, even though the boundary conditions are different. From these observations, it appears that the scalar transport at the interface is dominated by different mechanisms depending on the interfacial shear rate. For low shear rates that lead to patches, transport rates are related to parameters associated with these patches (patch area and patch residence time). For shear rates high enough to form streaks and bursts in the interface region, transport rates are obtained considering that the interfacial bursts/ejections govern the process. Both models show excellent predictions of the transport coefficients near the non-wavy gas–liquid interfaces.

1. INTRODUCTION

THE MECHANISM of heat and mass transport across gas–liquid interfaces is of great importance in numerous industrial and environmental processes. These include the design of many types of contacting equipment, e.g. boilers, condensers, evaporators, gas absorbers, pipelines, chemical reactors, nuclear reactors, and in other problems such as the aeration of rivers and the sea. In most cases of practical importance, the liquid flow is turbulent and the transport across the gas–liquid interface is governed by the liquid side. As a result, characteristics of turbulence in liquid flows near the interface are of significant value in understanding of the transport across the gas–liquid interfaces.

To date, there have been many attempts to model these processes and models of various complexity have been introduced. However, even the most sophisticated of these models rely on some kinds of hypotheses about the transport mechanism and require empirical inputs in the form of constants or functions. These models generally do not simulate the physical detail of the turbulence structure near the interface, but rather the overall effect of the turbulence on the mean flow. Therefore, the lack of understanding of the hydrodynamics and the transport mechanisms has resulted in many models short in accuracy and range of applicability. To better illustrate this point, let us review the analogous problem of gas absorption into a turbulent liquid flow.

In an early investigation, Lewis and Whitman [1] introduced the film model. In their model, they assumed that transport occurred across a film of laminar fluid adjacent to the interface in cases where the bulk fluid was turbulent. This led to a transfer coefficient that was proportional to the first power of the diffusivity, e.g. $K \propto \mathscr{D}$. However, mass transfer and heat transfer experiments later showed that the transfer coefficients varied as $\mathscr{D}^{2/3}$ at the fluid–solid boundaries and as $\mathscr{D}^{1/2}$ at the fluid–fluid boundaries. Furthermore, the concept of a steady transport across a laminar film was out of line with the experimental observations—particularly for the gas–liquid interfaces.

This led Higbie [2] to introduce the penetration/surface renewal model. He speculated that turbulence brought fluid from the bulk flow to the interface where unsteady absorption occurred into an essentially laminar fluid for a period T, after which the surface element was replenished with fresh bulk fluid. Unlike Lewis and Whitman's model where

$$K = \mathscr{D}/\delta \tag{1}$$

Higbie obtained

$$K = 2(\mathscr{D}/\pi T)^{1/2}. \tag{2}$$

Subsequently, Danckwerts [3] allowed for a random distribution of surface ages and showed

$$K = (\mathscr{D}/T)^{1/2} \tag{3}$$

where T may be thought of as the mean time between surface renewals. Other surface age distributions have also been introduced (Hanratty [4], amongst others),

† Permanent address: Department of Mechanical Engineering, Technion–Israel Institute of Technology, Haifa, Israel.

NOMENCLATURE

a_P	individual patch size area
A_P	total patch area at the interface
A_T	total interface area
D	equivalent diameter
$\mathscr{D}$	molecular diffusion coefficient
Fr	Froude number, $U_M/(gh)^{1/2}$
g	gravitational acceleration
h	mean flow depth
h^+	non-dimensional flow depth, $u_* h/\nu$
K	liquid phase mass transfer coefficient
Re	Reynolds number, $U_M h/\nu$
Re_D	Reynolds number, $U_M D/\nu$
Sc	Schmidt number, $\nu/\mathscr{D}$
T	time
T_B	mean time between bursts
T_E	mean time between ejections
T_P	mean patch residence time
u, v, w	streamwise, vertical, and spanwise fluctuating velocities
U_I	mean interface velocity
U_M	mean streamwise velocity
u_*	friction velocity, $(\tau/\rho)^{1/2}$
u'	r.m.s. of streamwise fluctuating velocity
x, y, z	streamwise, vertical, and spanwise coordinates
x^+	non-dimensional streamwise distance, $u_* x/\nu$
y^+	non-dimensional vertical distance, $u_* y/\nu$
z^+	non-dimensional spanwise distance, $u_* z/\nu$.

Greek symbols

δ	film thickness
ε	turbulent energy dissipation rate
λ	mean spanwise streak-spacing
λ^+	mean non-dimensional spanwise streak-spacing, $u_* \lambda/\nu$
Λ	integral length scale
ν	kinematic viscosity
ρ	density
τ	shear stress.

Subscripts

G	gas
I	gas–liquid interface
L	liquid
W	wall.

however they do not appear to lead to any significant improvement over those of Higbie and Danckwerts.

The surface renewal model, by giving a right dependence of K on $\mathscr{D}$ ($K \propto \mathscr{D}^{1/2}$) and introducing the effect of turbulence through a renewal rate parameter, later became a leading approach in many other models. Fortescue and Pearson [5] postulated that the transport across the interface is controlled by the large eddies of the size of the integral scale and the intensity of the bulk turbulent flow field. They proposed that the renewal time in the surface renewal model could be approximated by

$$T \approx \Lambda/u' \tag{4}$$

where Λ is the integral length scale and u' the r.m.s. of the streamwise velocity fluctuation.

On the other hand, Banerjee *et al.* [6] and subsequently Lamont and Scott [7] proposed a model in which the small eddies in the size of the Kolmogorov microscale controlled the transport across the interface. They suggested that

$$T = (\nu/\varepsilon)^{1/2} \tag{5}$$

where ε is the turbulent energy dissipation rate near the interface and ν the kinematic viscosity. Both the small eddy and large eddy models had some success in predicting some specific set of experimental data. However, they were unsupported by hydrodynamic measurements. Later, Theofanous [8] suggested that the small eddy model may be more relevant for the cases with high levels of turbulence, while the large eddy model works better when there is relatively low levels of turbulence.

In parallel to the surface renewal type models, the eddy diffusivity models were also introduced primarily by Levich [9] and later Davies [10]. The essence of such models is that the total diffusivity in the conservation equations is assumed to be the sum of a molecular diffusivity $\mathscr{D}$ and a turbulent eddy diffusivity $\varepsilon_{\mathscr{D}}$. A form of eddy diffusivity near the interface is generally suggested and the conservation equations are solved for the transport coefficients. Similarly, eddy diffusivity models of various complexity [11–13] have been proposed. However, these models, like all other models, are based on different simplifying assumptions regarding the turbulence dynamics and the controlling interfacial transport mechanism.

Although recent transfer experiments have added considerable empirical information on the problems (for a review of the subject, see Theofanous [8] and Rashidi [14]), for example, it is known that at relatively high Schmidt (or Prandtl) numbers, transfer rates across the interfaces into a turbulent liquid flow may be characterized by a transfer coefficient that varies as $\mathscr{D}^{1/2}$ where $\mathscr{D}$ is the molecular diffusivity. There are still many unanswered questions as to the actual dominating mechanism present near the interface.

Therefore, in order to properly model and hence predict the interfacial transport, turbulence characteristics near the interface must be understood. Unfortunately, experimental work on direct measurements of turbulent quantities near a gas–liquid interface has been very limited due to difficulties in making good measurements. It is only recently that Komori *et al.* [15], Nezu and Rodi [16], and Rashidi and Banerjee [17] were able to measure turbulence intensity near the shear-free gas–liquid interfaces. Both Komori *et al.* [15] and Nezu and Rodi [16] measured turbulence intensities in open channel flows but experienced some difficulties in examining the regions very close to the interfaces. Komori *et al.* [15] suggested that the surface is renewed by large energy containing eddies which are responsible for heat and mass transfer across the free surface. Their simultaneous velocity and temperature measurements showed that the large eddies which have renewed the free surface come back into the bulk flow to within deep distance from the free surface. However, they could not show the origin of the eddies and their effect on the transport across the interface. Rashidi and Banerjee [17], using a flow visualization technique, were able to make detailed measurements of the interface regions. These experiments showed the interaction of the wall bursts with the gas–liquid interface and consequently their dominating role in the process of interfacial transport. (Bursts are the lift off and break down of the streaky structures near a sheared boundary—wall or interface, in general each burst consists of several ejections.) Later, Komori *et al.* [18] further confirmed the importance of the wall bursts on transport across the interface. Their experiments showed that almost all the wall ejections reach the gas–liquid interface. Furthermore, the liquid mass transfer coefficient was found to be proportional to the square-root of the ejection frequency. As part of a continuing investigation, Rashidi and Banerjee [19, 20] further studied the turbulence structures in liquid layers as a shear was imposed on the gas–liquid interface by either countercurrent or cocurrent gas flow. These experiments showed the importance of the shear rate on the formation of the organized structures near either boundaries, i.e. the low-speed/high-speed streaks form and break down similarly near either walls or interfaces as shear rate is increased. These results are discussed in more detail in later sections.

In this paper, the mechanism of transport across the gas–liquid interfaces and the corresponding transport models have been studied as a function of shear rates. The overall objective is to better understand the process of heat and mass transfer across fluid–fluid interfaces with relevance to the dominant controlling hydrodynamics.

2. EXPERIMENTAL FACILITIES AND PROCEDURES

The experiments were conducted in a Plexiglas rectangular channel with gas and liquid flow facilities. The channel was made up of four equal sections and had dimensions of 4.0 m long, 0.20 m wide, and 0.15 m deep. It was designed so that at the test section, flow was fully developed with an aspect ratio large enough to be free from wall effects at the center. Figure 1 illustrates the experimental setup.

The liquid flow was provided by a centrifugal pump and was measured using a Venturi meter. The recirculating liquid flow was filtered continuously to remove solids larger than 5 μm. The gas flow was maintained through the use of two blowers in series. It was possible to impose a shear on the gas–liquid interface by flowing gas either cocurrent or countercurrent to the direction of the liquid stream. In order to measure the gas flow rate accurately, a rotary precision gas meter was used to monitor the flow during each run. Measurements of temperature were taken at the entrance, exit, and the test section of the channel using thermocouples placed on the side walls. These measurements were also monitored simultaneously with a set of precision mercury thermometers placed in the channel. Great care was taken to eliminate wave formation at the inlet and reflections from the outlet. As a result, the liquid flow was introduced into the inlet tank through several inlet holes in order to provide a setup that produced high flow rates with no significant interfacial waves. Similarly, the air flows were entered to the channel through a smooth flow duct equipped with a flow straightener to avoid interfacial instability that brings about waves. Efforts were also taken to maintain a constant average velocity and temperature throughout each run.

Measurements were made primarily in liquid streams by flow visualization. This was done through the use of very small ($\sim$20 μm in diameter) oxygen bubble tracers that were photographed using a high-speed video analyzer and alternatively a 35 mm camera with mechanically chopped flashes. The latter technique resulted in well-spaced traces of bubbles in a film frame from which velocities were found by image processing. The bubbles could be produced from two platinum wires (25 μm in diameter) using a high voltage pulse generator (generating 20–200 pulses s^{-1} with a pulse duration of 1–5 ms at up to 300 V). One wire was placed horizontally parallel to the bottom of the channel and aligned in the spanwise direction (and could be moved up and down between the wall and the interface), while the other wire was held vertically across the channel. Measurements of gas mean velocity were obtained using a multichannel (DISA56C01) hot wire anemometry system.

The high-speed video recording system was a two-camera Kodak (Spin Physics) EP-1000 Motion Analyzer. It was used with both conventional and fiber-optic synchronized-strobe units. The system had a maximum full screen capability of 1000 frames s^{-1} and a maximum split-screen capability of 6000 frames s^{-1}. The framing rate used in our experiments was generally 250 frames s^{-1}. The recorded data could be played back in slow motion as well as single frames

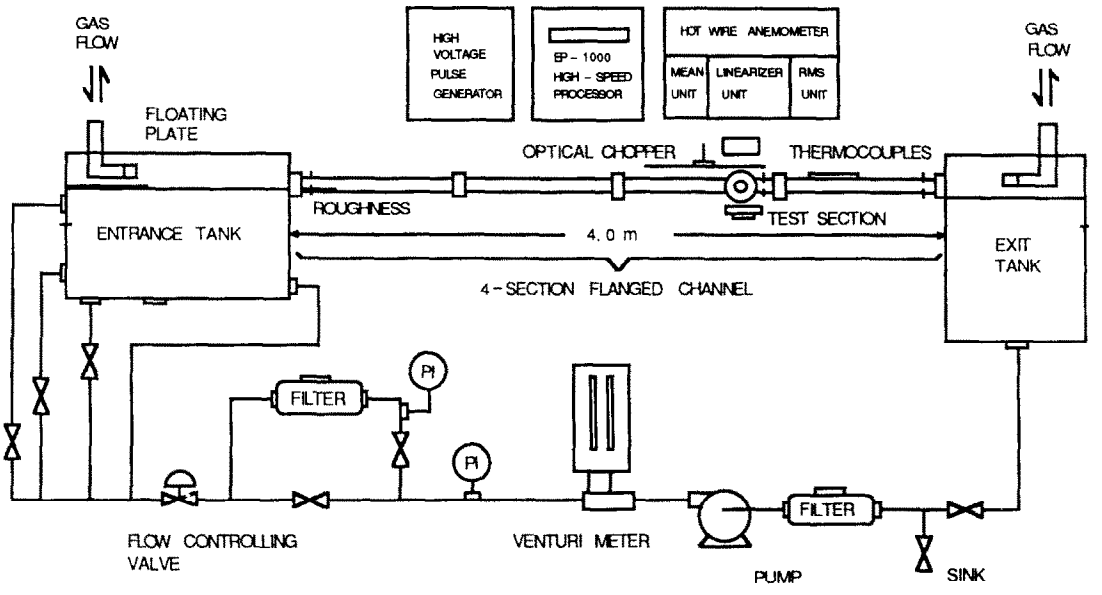

FIG. 1. Experimental facility and arrangement of measurement devices.

for detailed data analysis. The split-screen capability allowed one camera to be used to record the flow structures in the horizontal plane, while the other captured the structures in the vertical plane.

3. EXPERIMENTAL CONDITIONS

The experimental runs were conducted in the described facilities. The details of the experimental conditions are summarized in Tables 1–3. Three different cases were studied, (i) shear-free interfaces, (ii) countercurrently sheared interfaces, and (iii) cocurrently sheared interfaces. For the first case, experiments were conducted at four different liquid Reynolds (and Froude) numbers with no gas flows. In these cases the shear at the interface was negligible and these cases were considered to be shear free. However, for the two other cases, shear was imposed at the interface by either countercurrent or cocurrent flow of gas. Similarly, these experiments were carried out at four different liquid Reynolds (and Froude) numbers. The values of the wall and interface friction velocities were evaluated from the measured mean velocity profiles in these regions. For the runs discussed here, it was possible to impose shear at the interface with no significant interfacial waves. There-

Table 1. Shear-free interfaces

Run	Flow depth, h (cm)	Equivalent diameter, D (cm)	Mean velocity, U_M (cm s^{-1})	Interface velocity, U_i (cm s^{-1})	Friction velocity, u_{*w} (cm s^{-1})	Froude number, $Fr = (U_M/\sqrt{(gh)})$	Reynolds number, $Re = (U_M h/\nu)$	Reynolds number, $Re_D = (U_M D/\nu)$
1	2.75 ± 0.05	8.63	23.6 ± 2 3%	27.0	1.29	0.45	7500	24000
2	2.75	8.63	15.6	17.9	0.90	0.30	5000	16000
3	2.75	8.63	11.0	12.7	0.66	0.21	3500	11500
4	2.70	8.50	7.8	9.1	0.49	0.15	2500	8000

Table 2. Countercurrently sheared interfaces

Run	Liquid flow depth, h (cm)	Liquid mean velocity, U_M (cm s^{-1})	Liquid kinematic viscosity, ν (cm^2 s^{-1}) $\times 100$	Interfacial shear rate, (dU_M/dy) (s^{-1})	Liquid Froude number, $Fr = (U_M/\sqrt{(gh)})$	Liquid Reynolds number, $Re = (U_M h/\nu)$	Gas Reynolds number, $Re_G = (U_{MG} h_G/\nu_G)$
1	2.80 ± 0.05	23.2 ± 2 3%	0.858	9.1	0.44	7500	10600
2	3.25	13.2	0.848	29.5	0.23	5000	18400
3	2.95	10.2	0.848	26.0	0.19	3500	17600
4	2.85	7.4	0.839	25.2	0.14	2500	16600

Table 3. Cocurrently sheared interfaces

Run	Liquid flow depth, h (cm)	Liquid mean velocity, U_M (cm s^{-1})	Liquid kinematic viscosity, ν (cm^2 s^{-1}) $\times 100$	Interfacial shear rate (dU_M/dy) (s^{-1})	Liquid Froude number, $Fr = (U_M/\sqrt{(gh)})$	Liquid Reynolds number, $Re = (U_M h/\nu)$	Gas Reynolds number, $Re_G = (U_{MG} h_G/\nu_G)$
1	2.80±0.05	23.2±2–3%	0.867	11.1	0.44	7500	16600
2	3.25	13.2	0.848	27.2	0.23	5000	19800
3	2.95	10.2	0.848	25.5	0.19	3500	19200
4	2.85	7.4	0.839	24.1	0.14	2500	16600

fore, the effect of turbulence on transport was studied without the influence of interfacial waves.

4. TRANSPORT MECHANISMS AS A FUNCTION OF SHEAR RATE

4.1. *Shear-free interfaces*

In order to investigate the dominant structures near the wall and their interactions with the gas–liquid interface, the high-speed video system was employed. The system was used to view simultaneously the near wall structures in the horizontal plane (upper portion of the screen) and their lift-up and break down 'bursts' in the vertical plane (lower portion of the screen). Figure 2 illustrates the sequence of pictures obtained in this way for Run 2 in Table 1. As it appears from these pictures and many other video sequences, the bursts originating at the wall clearly lift up, interact with the interface, and then return and mix into the bulk flow. Furthermore, it seems as these events give rise to the formation of 'renewed surface patches' at the interface.

The formation of surface patches at the interface was further examined by placing the horizontal wire right at the interface and visualizing the free surface with oxygen bubble tracers. Figure 3 illustrates the visualization of the interface this way. As it is seen from this figure and video sequences, the interfacial patches are indeed formed from the interaction of the wall bursts with the interface. This was observed for all the experimental runs. The finding is of great significance, since it illustrates the dominating role of the wall organized structures in the transport across the interface.

The study of near wall structures dates back to the systematic investigation of Kline *et al.* [21]. They found through a series of flow visualization experiments using hydrogen bubbles that even at $y_W^+ = 2.7$ the bubbles did not follow straight trajectories and they accumulated into an alternating array of low-speed and high-speed regions called 'streaks'. It was observed that these structures periodically lifted off, oscillated, then became unstable and broke up chaotically. The repeated cycle of events ended with an insweep or inrush of fresh fluid to replace the ejected fluid in the wall region. Kim *et al.* [22] showed that virtually all of the net production of turbulent energy

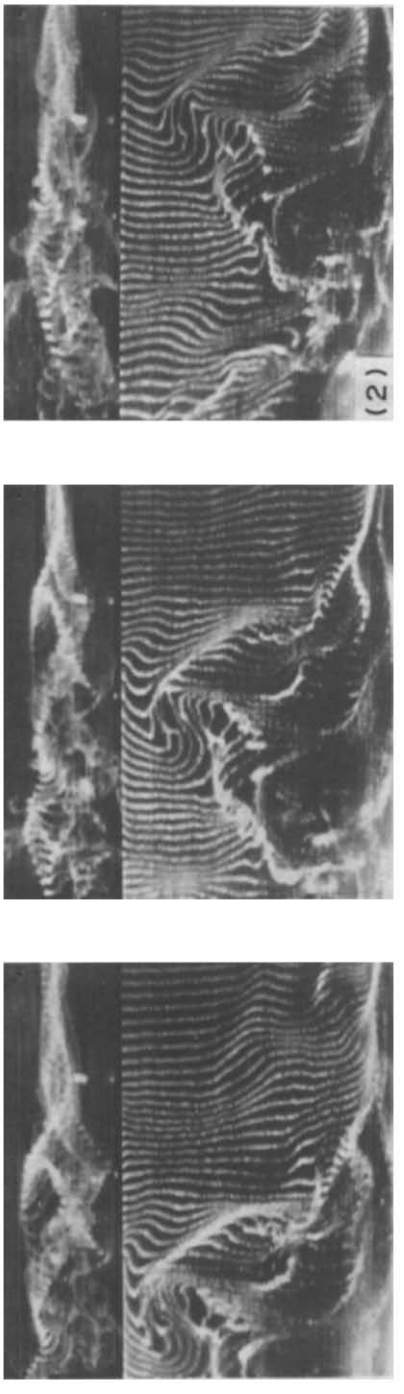

FIG. 2. Sequential pictures of wall burst interaction with the interface (Run 2).

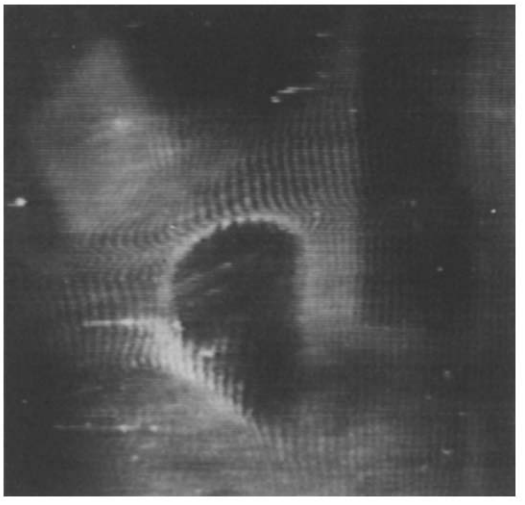

FIG. 3. Illustration of interfacial patches formed as a result of burst renewal of the interface (Run 2).

for the range $0 < y_W^+ < 100$ occurs during the lifting and break down of these streaks. Both ejection and insweep events have been shown by many authors to be extremely important and contributing to as much as 60–80% of the production of Reynolds stress.

The characteristics of streak formation and break down near the wall have been studied by many investigators (most recently Smith and Metzler [23] and Rashidi and Banerjee [19, 20]). It has been found that the mean streak spacing, λ, can be best scaled in terms of the wall variables: shear velocity u_{*W} and kinematic viscosity ν. The mean spacing nondimensionalized in these units changes very little with Reynolds number and exhibits consistent values of

$$\lambda^+ = (\lambda u_{*W}/\nu) \approx 100 \tag{6}$$

at $y_W^+ = 5$. Figure 4 illustrates the low-speed/high-speed streaks visualized by means of oxygen bubbles at several distances from the wall. As seen from these pictures the streak-spacing increases with increased distance from the wall. This increase is caused by the two effects of fluttering and merging of the low-speed streaks. Rashidi and Banerjee also measured the wall ejection and burst frequencies. These measurements have shown that the burst frequencies in the wall region are best scaled with the inner wall variables. In terms of inner variables, the non-dimensional mean time between bursts was given by

$$T_B^* = (u_{*W}^2/\nu) T_B \approx 85. \tag{7}$$

Turning back now to the interaction of the wall ejections and the interface, the characteristics of the surface patches were further studied from the video sequences. For each run, a video sequence of at least 22 000 frames ($\sim$3 min) was recorded. From this sequence, 200 frames were analyzed. The measurements of patch area and number were carried out from individual still pictures with each picture about 0.4 s apart. (The values of patch area A_P were determined over a total area A_T of streamwise length

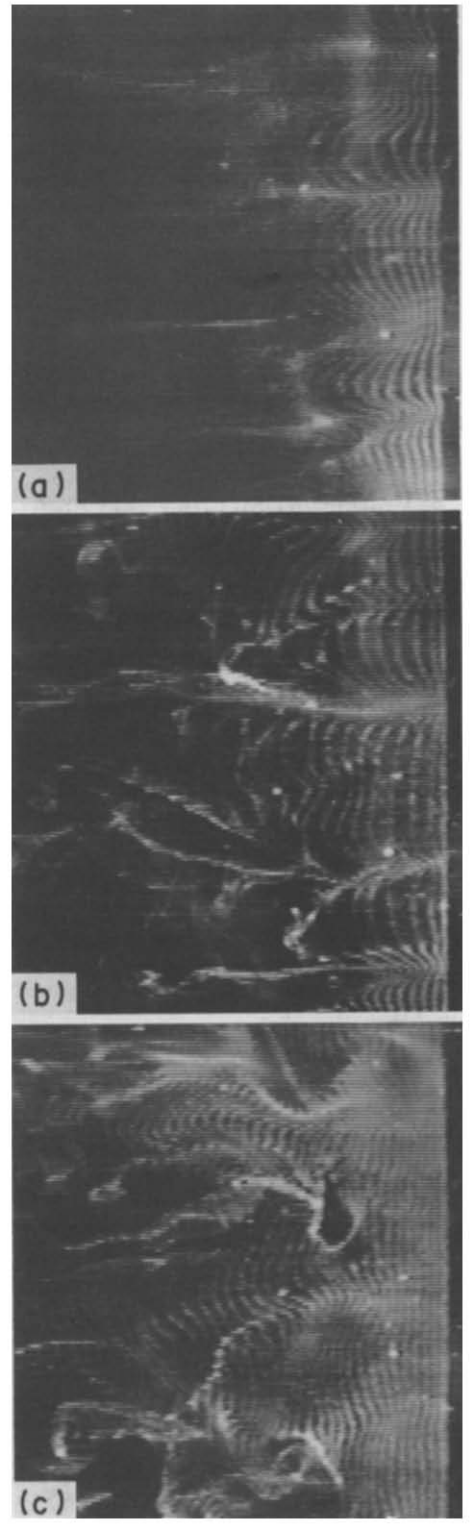

FIG. 4. Low-speed/high-speed streaks at various distances from the wall, Run 2: (a) $y_W^+ = 5$; (b) $y_W^+ = 20$; (c) $y_W^+ = 40$.

$L = U_I T_P$ and an arbitrary width, where T_P is the mean patch residence time and U_I the mean streamwise velocity at the interface.) This was generally done twice independently. Figure 5 shows the typical

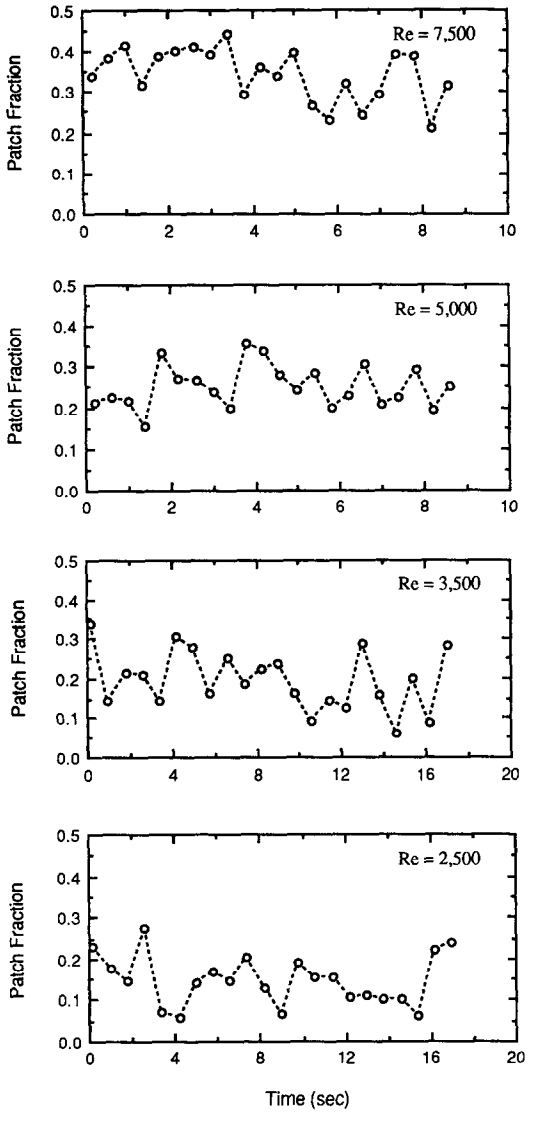

FIG. 5. Variation of dimensionless total patch area, A_P/A_T, with time.

variation of the surface patch fraction as a function of time for all the experimental runs in Table 1. Figure 6 illustrated the dimensionless mean total patch area and patch size as a function of Reynolds number. As seen from these plots, the total patch area at the interface increases with increase in Reynolds number. However, the individual patch size decreases as Reynolds number is increased. This implies that as Reynolds number increases, the number of wall ejections would also increase. On the other hand, the size of energy containing eddies reaching the interface would decrease. This indeed agrees with the previous findings [19]. Namely, the wall ejection frequency increases with Reynolds number, while the low-speed streak spacing decreases as Reynolds number is increased. Therefore, the increase in ejection frequency and the decrease in streak-spacing with Reynolds number lead to the results observed near the interface, since the

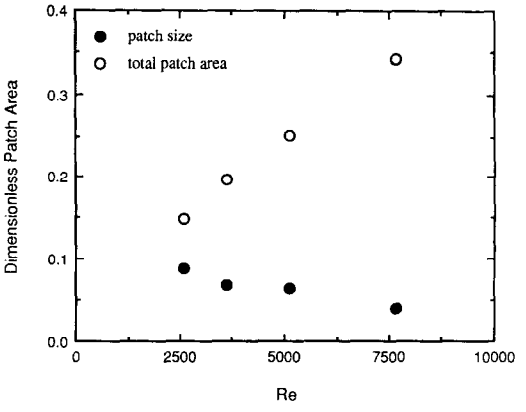

FIG. 6. Effect of Reynolds number on dimensionless mean patch size and total patch area, a_P/A_T and A_P/A_T.

ejection sites are more closely spaced and the rate of ejection is also enhanced.

The values of patch residence time and patch frequency were also evaluated from the video sequences. Figure 7 illustrates the comparison of the patch renewal frequency with the wall burst frequency. As it is seen from this figure, about 76% of the wall bursts reach the interface. This is lower than the 90% value found by Komori *et al.* [18]. Komori *et al.* [18] measured the renewal frequency from the concentration fluctuations near the interface. Since their concentration probe was slightly below the interface, their renewal frequency may be an overestimate.

The measurements of patch residence time T_P were obtained from the vertical plane-view video sequence (about 4–5 times longer in length than the picture in Fig. 2). The value of T_P corresponds to the difference in the initial time when wall ejections first reach the interface and the final time when these structures first roll down toward the wall and away from the interface. Similarly, these values were averaged, taking about 200 measurements of patch residence time for each run. Equation (8) describes the variation of the patch residence time measured this way as a function of Reynolds number

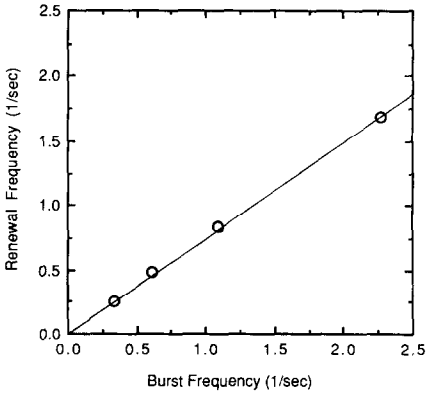

FIG. 7. Comparison of patch renewal frequency with wall burst frequency.

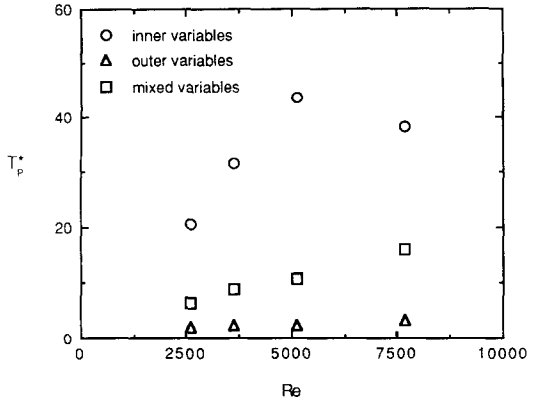

FIG. 8. Effect of Reynolds number on average patch residence time nondimensionalized with inner, outer and mixed variables. ○, inner variables $[T_P^* = (u_*^2/\nu)T_P]$; Δ, outer variables $[T_P^* = (U_M/h)T_P]$; □, mixed variables $[T_P^* = (U_M u_*^2/h\nu)^{1/2}T_P]$. The uncertainty in the values of T_P^* is ±8% at the 95% confidence level for about 200 measurements.

$$T_P = 61.12\ Re^{-0.568}. \tag{8}$$

As seen from this equation, the mean patch residence time decreases with the increase in the Reynolds number.

Figure 8 shows the patch residence time scaled by inner variables, outer variables, and mixed variables. It appears that none of these scales gives perfect collapse of the data as a function of Reynolds number, i.e. the Reynolds number dependence is not completely removed. The best scaling is, in fact, obtained with u_{*W} and h

$$(T_P u_{*W}/h) \approx 0.15. \tag{9}$$

The ratio u_{*W}/h is related to the time the burst is acted on by the mean flow. This in turn determines the burst trajectory and velocity when it reaches the interface and hence the time of interaction with the interface.

Once again examining the result obtained in Fig. 6 and recalling that the fractional patch area is based on the area swept by a surface flow of unit width in one average patch residence time, one can investigate the scaling of A_P/A_T. It can be expected that the fractional patch area, A_P/A_T, will be a function of burst frequency, surface velocity and patch residence time. Therefore, it involves both inner and outer variables as well as T_P. Indeed, such a relationship is found in that

$$(A_P/A_T)[(h\nu/U_M u_{*W}^2)^{1/2}(1/T_P)] \approx 0.02. \tag{10}$$

The term in square brackets on the left-hand side of equation (10) is the inverse of the patch residence time scaled with mixed variables. It should be noted that the scaling results are limited to the range of Reynolds numbers in the present experiment.

4.2. *Interfaces with shear*

In the previous section, discussion was focused on the transport mechanisms near shear-free interfaces. However, in many cases of interest shear is imposed at the interface by the relative motion between the fluids on each side. It is of significant importance to see whether the streaks and bursts form at the fluid–fluid interfaces when shear is imposed, and if so how they compare qualitatively and quantitatively to those seen near the walls.

Rashidi and Banerjee [19] tackled this problem in detail. Their experiments indeed showed that the low-speed/high-speed streaks form in the region very close to the interface if shear is imposed on the liquid surface by motion of a gas. Even though the boundary conditions at the wall and at the interface were different, the main characteristics of the streaks appeared similar. The spanwise spacing of the streaks when non-dimensionalized using the interfacial shear velocity, u_{*I}, and kinematic viscosity, ν, was about 100 units (similar to the spacing of the wall streaks)

$$\lambda^+ = (\lambda u_{*I}/\nu) \approx 100. \tag{11}$$

The ejections and break down of the streaks also showed similar features to the ones near the wall. Figure 9 illustrates the generation of bursts near the wall and near the sheared gas–liquid interfaces. It was found from these experiments that the ejections and burst frequencies scale on local inner variables and the numerical values in non-dimensional frequency units are about the same whether the bursts or ejections originate near the interface or near the wall. In terms of inner variables, the non-dimensional mean time between bursts and ejections were

$$T_B^* = (u_{*I}^2/\nu)T_B \approx 87 \tag{12}$$

$$T_E^* = (u_{*I}^2/\nu)T_E \approx 38. \tag{13}$$

These experiments showed that the shear rate has the main influence on the phenomena and the effect of boundary conditions is much less important.

The effect of shear rate on the transition of the interface structures from the patches to the streaks was also investigated. Our experiments show that the critical shear rate for the formation of streaks is between 8 and 10 s^{-1}. Below this shear rate, the patch structures dominate the interface, whereas above this shear rate, the streaky structures replace the patches. The numerical study of Lam and Banerjee [24] has shown that the transition point can be best described by the non-dimensional shear rate

$$[\overline{uv}(dU_M/dy)/\varepsilon] \approx 1.0 \tag{14}$$

where dU_M/dy is the shear rate, $\overline{uv}$ the Reynolds stress, and ε the rate of turbulent dissipation. If the left-hand side of equation (14) exceeds unity then the streak structures appear, whereas otherwise they do not.

5. TRANSPORT RATES AS A FUNCTION OF SHEAR RATE

5.1. *Non-wavy shear-free interfaces*

In light of the experimental observations and the penetration/surface renewal theories, a patch renewal

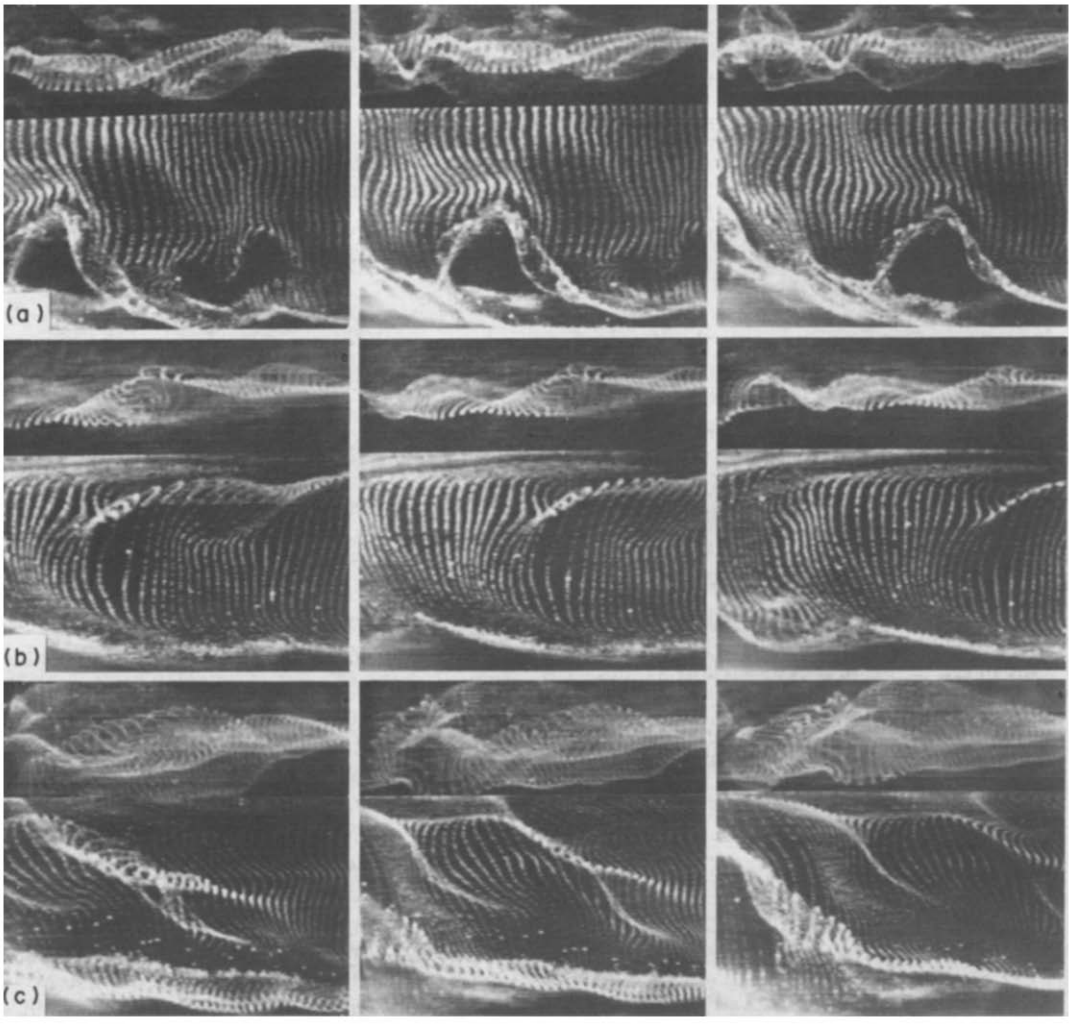

FIG. 9. Sequential pictures of bursts near wall and near sheared gas–liquid interfaces. (a) near wall: shear-free interface; (b) near interface: countercurrently sheared interface; (c) near interface: cocurrently sheared interface. The lower part of each picture is a side view and the upper part is a plan view of the same structure.

model for the prediction of the liquid transfer coefficient at the shear-free interfaces is proposed. In this model, it is conjectured that the process of transport across the non-wavy shear-free interfaces is controlled by the ejections evolving from the wall. These ejections are seen (from the video sequences in previous sections) to reach the interface and form renewed surface patches that are considered to be the dominating regions in the interfacial heat and mass transport (the non-patchy area contributes very little to the transport). It is further assumed that for the Reynolds numbers studied here the small scale fluctuations in the patches can be ignored. Therefore, the average transfer coefficient is defined as

$$K = (A_P/A_T)(\mathscr{D}/T_P)^{1/2} \tag{15}$$

where A_P/A_T is the mean patch fraction at the interface, $\mathscr{D}$ the molecular diffusion coefficient, and T_P the mean patch residence time.

Substituting equations (9) and (10), one obtains the following general equation for the average transfer coefficient at the shear-free non-wavy interfaces

$$\frac{K\,Sc^{1/2}}{(U_M u_{*w})^{1/2}} = 0.0077. \tag{16}$$

Figure 10 shows the comparison of the transfer coefficients calculated from equation (16) with the value measured by Komori *et al.* [18]. As seen from this figure, there is an excellent agreement between the patch renewal model and Komori *et al.*'s data. It should be noted that the scaling laws for T_P and A_P/A_T implicit in equation (16) have been tested only for $Re_D < 40\,000$. Therefore, the range of applicability of equation (16) may be limited to these Reynolds numbers.

5.2. *Non-wavy interfaces with shear*

As the shear rate is increased at the interface (the left-hand side of equation (14) exceeds 1.0), the patchy

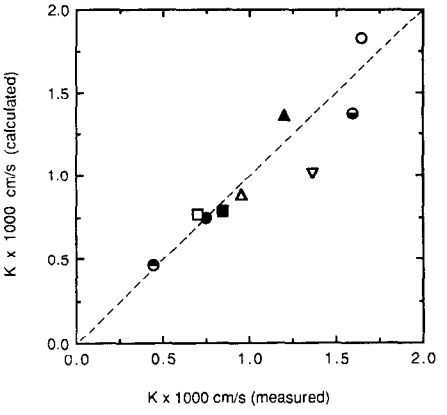

FIG. 10. Comparison of the transfer coefficients (shear-free interfaces) calculated from equation (16) with measured values by Komori *et al.* [18]. Symbols have the same meaning as in Komori *et al.* [18].

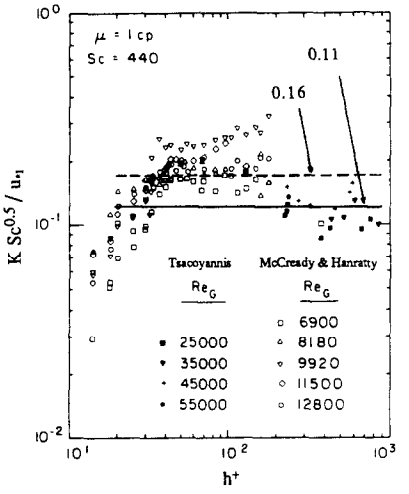

FIG. 11. Comparison of the transfer coefficients (interfaces with shear) calculated from equation (20) with measured values by McCready and Hanratty [25] and Tsacoyannis [26].

structures are replaced by the streaks and bursts. It was observed that the interface regions become the sites of frequent ejections. Furthermore, it was seen that the interface region becomes relatively quiescent between the ejections, so that finer scales are unlikely to affect the transport processes. With these considerations, one can define the transport coefficient as before

$$K = (\mathscr{D}/T)^{1/2} \tag{17}$$

where T is the mean time between ejections or bursts. Rearranging equation (17)

$$\frac{K\,Sc^{1/2}}{u_{*l}} = \left(\frac{\nu}{Tu_{*l}^2}\right)^{1/2}. \tag{18}$$

As it was shown in Section 4.2, the mean time between ejections and burst scales with the local shear velocities and the liquid kinematic viscosity. While it is not clear from these considerations whether ejections or bursts are the dominant transport mechanism, the relevant period lies somewhere between

$$T^* = (u_{*l}^2/\nu)T = 38 \text{ to } 87. \tag{19}$$

Substituting these results in equation (18), one obtains

$$\frac{K\,Sc^{1/2}}{u_{*l}} = 0.11 \text{ to } 0.16. \tag{20}$$

It is interesting to note that in contrast to the expression for the shear-free interfaces given by equation (16) which has mixed scaling of u_{*w} and U_M, equation (20) is only scaled by inner variable u_{*l}. Equation (20) should hold as long as the shear rate is high enough to form the streaky structures at the interface as determined by equation (14). Figure 11 shows the comparison of the transport data for flows with interfacial shear from McCready and Hanratty [25] and Tsacoyannis [26] with equation (20). It appears from this figure that the present model has a good agreement with the experimental measurements for $h^+ > 40$.

It should be noted that the transport data obtained in these experiments were not completely wave free. For instance, at $h^+ = 100$, the r.m.s. wave amplitude was about 0.3 mm on a film of average thickness of 62 mm. McCready and Hanratty [25] and later Back and McCready [27] attempted to explain the transfer rates through the measurements of interfacial waves. It is remarkable to note that our measured ejection frequency at the interface corresponds closely to the peak in their wave energy spectrum. Since the ejections dominate the transfer process, it is possible that the maximum amplitude waves are due to these ejections and as a result the transfer coefficients could also be explained in terms of the measured wave spectra. Clearly, in order to verify this point the wave-turbulence interactions need to be further investigated.

6. CONCLUSIONS

Mechanisms of transport at non-wavy fluid–fluid interfaces have been studied. It has been shown that the controlling mechanism near boundaries (interface or wall) is governed by the shear rate. A shear rate criterion has been proposed that describes the onset of streaks and their break down into ejections and bursts.

At low interfacial shear rates, when streaks and ejections do not occur at the interface the mechanism of interfacial transport is dominated by the ejections generated at the wall. The wall ejections are seen to reach the interface, form renewed surface patches, return and mix into the bulk flow. The transfer rates are well predicted by considering only these patch areas as active in transport. The transfer coefficients are predicted to scale with wall shear velocity and mean velocity and the agreement with experiments is good. At high interfacial shear rates, when streaks and ejections occur at the interface, the transport

mechanism is dominated by the ejections and bursts generated at the interface. The transfer coefficients are well predicted by equation (20), indicating that the coefficients scale with interfacial shear velocity. The agreement with experiments is also good.

Acknowledgement—We would like to express our gratitude to the U.S. Department of Energy, Basic Energy Sciences Program, for support of this project through Grant No. DE-FG03-85ER13314.

REFERENCES

1. W. K. Lewis and W. G. Whitman, Principles of gas absorption, *Ind. Engng Chem.* **16**, 1215–1220 (1924).
2. R. Higbie, The rate of absorption of a pure gas into a still liquid during short periods of exposure, *Trans. A.I.Ch.E.* **31**, 365–388 (1935).
3. P. V. Danckwerts, Significance of liquid-film coefficients in gas absorption, *Ind. Engng Chem.* **43**, 1460–1467 (1951).
4. T. J. Hanratty, Turbulent exchange of mass and momentum with a boundary, *A.I.Ch.E. Jl* **2**, 359–362 (1956).
5. G. E. Fortescue and J. R. Pearson, On gas absorption into a turbulent liquid, *Chem. Engng Sci.* **22**, 1163 1176 (1967).
6. S. Banerjee, E. Rhodes and D. S. Scott, Mass transfer to falling wavy liquid films in turbulent flow, *Ind. Engng Chem. Fundam.* **7**, 22–27 (1968).
7. J. C. Lamont and D. S. Scott, An eddy cell model of mass transfer into the surface of a turbulent liquid, *A.I.Ch.E. Jl* **16**, 513–519 (1970).
8. T. G. Theofanous, Conceptual models of gas exchange. In *Gas Transfer at Water Surfaces* (Edited by W. Brutsaert and G. H. Jirka), pp. 271–281. Reidel/North-Holland, Amsterdam (1984).
9. V. G. Levich, *Physiochemical Hydrodynamics*. Prentice-Hall, Englewood Cliffs, New Jersey (1962).
10. J. T. Davies, *Turbulence Phenomena*. Academic Press, New York (1972).
11. A. F. Mills and D. K. Chung, Heat transfer across turbulent falling films, *Int. J. Heat Mass Transfer* **16**, 694–696 (1973).
12. G. Y. Lee and W. N. Gill, A note on velocity and eddy viscosity distributions in turbulent shear flows with the free surfaces, *Chem. Engng Sci.* **32**, 967–979 (1977).
13. S. A. Kitaigorodskii and M. A. Donelan, Wind-wave effects on gas transfer. In *Gas Transfer at Air–Water Surfaces* (Edited by W. Brutsaert and G. H. Jirka), pp. 147–170 (1984).
14. M. Rashidi, Turbulence structure and transport mechanisms in liquid streams bounded by a wall and a gas–liquid interface, Ph.D. Thesis, University of California (1989).
15. S. Komori, H. Ueda, F. Ogino and T. Mizushina, Turbulence structure and transport mechanism at the free surface in an open channel flow, *Int. J. Heat Mass Transfer* **25**, 513–521 (1982).
16. I. Nezu and W. Rodi, Open-channel flow measurements with a laser Doppler anemometer, *J. Hydraul. Engng* **112**, 335–355 (1986).
17. M. Rashidi and S. Banerjee, Turbulence structure in free surface channel flows, *Physics Fluids* **31**, 2491–2503 (1988).
18. S. Komori, Y. Murakami and H. Ueda, The relationship between surface-renewal and bursting motions in an open-channel flow, *J. Fluid Mech.* **203**, 103–123 (1989).
19. M. Rashidi and S. Banerjee, The effect of boundary conditions and shear rate on streak formation and breakdown in turbulent channel flows, *Physics Fluids A* **2**(10), 1827–1838 (1990).
20. M. Rashidi and S. Banerjee, Streak formation and breakdown near boundaries in turbulent open channel flow, *J. Fluids Engng* **112**, 164–170 (1990).
21. S. J. Kline, W. C. Reynolds, F. A. Schraub and P. W. Runstadler, The structure of turbulent boundary layers, *J. Fluid Mech.* **70**, 741–773 (1967).
22. H. T. Kim, S. J. Kline and W. C. Reynolds, The production of turbulence near a smooth wall in a turbulent boundary layer, *J. Fluid Mech.* **50**, 133–160 (1971).
23. C. R. Smith and S. P. Metzler, The characteristics of low-speed streaks in the near-wall region of a turbulent boundary layer, *J. Fluid Mech.* **129**, 27–54 (1983).
24. K. Lam and S. Banerjee, On the condition of streak formation in a bounded turbulent flow, *Physics Fluids* (1991), submitted.
25. M. J. McCready and T. J. Hanratty, Effect of air shear on gas absorption by a liquid film, *A.I.Ch.E. Jl* **31**, 2066–2074 (1985).
26. Y. Tsacoyannis, A study of gas absorption into liquids in turbulent stratified flow, These de Docteur-Ingenieur, Université Paul Sabatier de Tolouse (1976).
27. D. D. Back and M. J. McCready, Effect of small-wavelength waves on gas transfer across the ocean surface, *J. Geophys. Res.* **93**, 5143–5152 (1988).

MECANISMES DU TRANSPORT DE CHALEUR ET DE MASSE AUX INTERFACES GAZ–LIQUIDE

Résumé—On étudie le transport interfacial dans les écoulements turbulents liquides en panache. Les expériences de visualisation montrent que la structure turbulente près des frontières (interface ou paroi) est gouvernée par les contraintes de cisaillement. Pour les faibles valeurs de celles-ci des "cellules" sont observées aux interfaces qui proviennent d'éjections créées au voisinage de la paroi. Ces éjections arrivent à l'interface, où se forment de nouvelles cellules qui retournent dans le coeur de l'écoulement où elles se mélangent. Pour les grandes valeurs du cisaillement interfacial, se forment à l'interface des filets faible vitesse/grande vitesse lesquels se brisant en "bouffées". Les structures des filets et bouffées sont semblables à celles observées près de la paroi, même si les conditions aux limites sont différentes. De ces observations, il apparait que le transport scalaire à l'interface est dominé par différents mécanismes dépendants du taux de cisaillement interfacial. Pour les faibles taux qui conduisent aux cellules, le transport est relié aux paramètres associés à ces cellules (surface et temps de séjour des cellules). Pour les taux élevés qui conduisent aux filets et aux bouffées dans la région interfaciale, le transport est analysé en considérant que les bouffées interfaciales et les éjections gouvernent le processus. Les deux modèles montrent des prédictions excellentes des coefficients de transport près des interfaces gaz–liquide non ondulés.

MECHANISMEN DER WÄRME- UND STOFFÜBERTRAGUNG AN GAS/FLÜSSIGKEITS-GRENZFLÄCHEN

Zusammenfassung—Die Transportvorgänge in turbulenten Flüssigkeitsströmungen werden in einem Gerinne untersucht. Experimente mit einer Sichtbarmachung der Strömung zeigen, daß die Turbulenzstruktur nahe den Berandungen (an der Grenzfläche oder an der Wand) von der Schubkraft bestimmt wird. Bei kleinen Werten der Schubkraft an der Grenzfläche werden besondere Flächenbereiche beobachtet, die durch Abströmvorgänge nahe der Wand entstehen. Es ist zu beobachten, daß die Abströmungen die Grenzfläche erreichen, derartige Oberflächenbereiche bilden, dann umkehren und sich mit der Hauptströmung wieder vermischen. Bei großen Werten der Schubkraft an der Grenzfläche bilden sich hier Streifen mit geringer und mit hoher Geschwindigkeit, die dann wieder zusammenbrechen. Die qualitativen Eigenschaften dieser Streifen und ihres Verhaltens beim Zusammenbruch sind ähnlich denjenigen, die nahe an der Wand beobachtet werden—obwohl die Randbedingungen unterschiedlich sind. Aus diesen Beobachtungen wird gefolgert, daß der skalare Transport an der Grenzfläche je nach Schubkraft von unterschiedlichen Mechanismen gesteuert wird. Bei kleiner Schubkraft, wenn sich die typischen Oberflächenbereiche einstellen, hängt der Transport von diesbezüglichen Parametern ab (Fläche dieser Bereiche und deren Lebensdauer). Sofern die Schubkraft für die Bildung der beschriebenen Streifen an der Grenzfläche ausreicht, ergibt sich das Transportverhalten aus der Betrachtung der Vorgänge beim Zusammenbruch der Streifenströmung. Beide Modelle sind in der Lage, die Transportkoeffizienten in der Nähe einer wellenfreien Gas/Flüssigkeits-Grenzfläche vorauszusagen.

МЕХАНИЗМЫ ТЕПЛО- И МАССОПЕРЕНОСА У ГРАНИЦ РАЗДЕЛА ГАЗ–ЖИДКОСТЬ

Аннотация—Исследуется межфазный перенос при турбулентных течениях жидкости в подводящих каналах. Эксперименты по визуализации течения показывают, что структура турбулентност и вблизи границ (межфазной границы или стенки) определяется скоростью сдвига. При низких значениях скорости сдвига на межфазной границе наблюдаются "пятна", образующиеся из выбросов вблизи стенки. Выбросы достигают межфазной границы, возобновляют пятна на поверхности, возвращаются и смешиваются с объемным потоком. В случае высоких значений скорости сдвига на межфазной границе формируются низко- или высокоскоростные конвекционные токи, которые взрывообразно разрушаются. Наблюдения свидетельствуют о том, что перенос у межфазной границы осуществляется по различным механизмам в завимости от скорости сдвига. При низких скоростях сдвига, которые приводят к образованию пятен, скорости переноса связаны с параметрами, характеризующими эти пятна (площадь пятна и время его существования). В случае же скоростей сдвига, достаточно высоких для образования конвекционных токов и взрывов в области межфазной границы, скорости переноса определяются с учетом того факта, что процессом управляют взрывы или выбросы на межфазной границе. Обе модели позволяют точно рассчитывать коэффициенты переноса вблизи неволнистых границ раздела газ–жидкость.